



Supplementary Information for Multicolor 3D MINFLUX nanoscopy of mitochondrial MICOS proteins

Jasmin K. Pape^{a,1}, Till Stephan^{a,b,1}, Francisco Balzarotti^{a,2}, Rebecca Büchner^a, Felix Lange^{a,b}, Dietmar Riedel^c, Stefan Jakobs^{a,b,3} and Stefan W. Hell^{a,d,3}

^a Department of NanoBiophotonics, Max Planck Institute for Biophysical Chemistry, 37077 Göttingen, Germany

^b Clinic of Neurology, University Medical Center Göttingen, 37075 Göttingen, Germany

^c Laboratory of Electron Microscopy, Max Planck Institute for Biophysical Chemistry, 37077 Göttingen, Germany

^d Department of Optical Nanoscopy, Max Planck Institute for Medical Research, 69120 Heidelberg, Germany

¹ These authors contributed equally to this work.

² Present address: Research Institute of Molecular Pathology, Vienna Biocenter, Vienna 1030, Austria.

³ To whom correspondence may be addressed:

Stefan Jakobs, Department of NanoBiophotonics, Max Planck Institute for Biophysical Chemistry, Am Fassberg 11, 37077 Göttingen, Germany, +49-551-201-2531, sjakobs@gwdg.de

Stefan W. Hell, Department of NanoBiophotonics, Max Planck Institute for Biophysical Chemistry, Am Fassberg 11, 37077 Göttingen, Germany, +49-551-201-2500, shell@gwdg.de

This PDF file includes:

- Supplementary text
- Figures S1 to S7
- Legends for Movies S1 to S7
- SI References

Other supplementary materials for this manuscript include the following:

- Movies S1 to S7

Materials and Methods

Sample preparation

Labeling of primary antibodies

We labeled primary antibodies directly using amine-reactive crosslinker chemistry at the primary amines of the lysine side chains natively present in the antibodies. To this end, we purified the antibodies using a centrifugal concentrator (Vivaspin 500, MWVO 10.000, Sartorius, Göttingen, Germany) and re-solved them in PBS (pH 7.4), resulting in an amount of roughly 200 µg of antibody at a concentration of 1 µg/µl. We added 20 µl NaHCO₃ (1 M, pH 8.3–8.5) to the solution and supplied about 20 µg of the commercially available 1-Hydroxy-2,5-pyrrolidinedione (NHS) ester derivative of the fluorescent dye (Alexa Fluor 647 NHS Ester, A37573, Thermo Fisher Scientific, Waltham, MA, USA; CF660C Succinimidyl Ester, 92137 and CF680 Succinimidyl Ester, 92139, both Biotium, Inc., Fremont, CA, USA) solved in dimethylformamide (DMF) at a concentration of 10 mg/ml. The solution was protected from light and incubated at room temperature for 1–2 h while gently stirring. For purification, we pre-washed a gel filtration column (PD MiniTrap G-25, GE Healthcare Life Sciences, Little Chalfont, Buckinghamshire, United Kingdom) several times with PBS (pH 6.5) before adding the antibody solution and eluting again with PBS (1x, pH 6.5). A fraction of 200 µl was collected and the protein concentration verified using a micro-volume spectrometer (NanoDrop, Thermo Fisher Scientific, Waltham, MA, USA). We used antibodies against Mic60 (Proteintech, Rosemont, IL, USA) labeled with Alexa Fluor 647 and CF660C, respectively, against the FLAG-tag (Sigma Aldrich, St. Louis, MO, USA) and against Mic19 (Atlas antibodies, Bromma, Sweden), both conjugated to CF680 and an antibody against ATPB (abcam, Cambridge, United Kingdom) labeled with Alexa Fluor 647.

Cell culture

HeLa cells (1) (CCL-2, verified by ATCC cell line authentication service) and human primary dermal fibroblasts (HDFa, ATCC, Manassas, VA, USA) were cultured in DMEM containing 4.5 g/l glucose and GlutaMAX™ additive (Thermo Fischer Scientific, Waltham, MA, USA). The growth medium was further supplemented with 100 U/ml penicillin and 100 µg/ml streptomycin (Merck Millipore, Burlington, MA, USA), 1 mM sodium pyruvate (Sigma Aldrich, St. Louis, MO, USA) and 10% [v/v] fetal bovine serum (Merck Millipore, Burlington, MA, USA). The U-2 OS cells (ATCC, Manassas, VA, USA) were cultured in McCoy's medium (Thermo Fischer Scientific, Waltham, MA, USA). Cells seeded on coverslips two days prior to fixation were incubated at 37 °C and 5% CO₂. For imaging of Mic10 we used a Mic10-TO HeLa cell line, where a Mic10-FLAG fusion protein replaced the endogenous Mic10 (2). To this end, we integrated Mic10 C-terminally fused with a FLAG-T2A-EGFP tag into the genome of HeLa Mic10 knockout cells under the control of a tetracycline-dependent (TetOn) promoter. Induction with doxycycline led to the expression of the fusion protein. The self-cleaving T2A-peptide (3) caused the release of cytosolic green fluorescent protein (EGFP) as an expression reporter, whereas the FLAG-tagged Mic10 was transported into the mitochondria. We induced Mic10-TO HeLa cells for Mic10-FLAG expression by adding DMEM containing 0.025 µg/ml doxycycline hydulate (Sigma Aldrich, St. Louis, MO, USA) for 24 h.

Staining

Before labeling, we fixed the cells by adding 2 ml of a pre-warmed solution (37 °C) of 8% formaldehyde in PBS (137 mM NaCl, 2.68 mM KCl and 10mM Na₂HPO₄, pH 7.4) to 2 ml DMEM culture medium. After 5 minutes we exchanged the solution for 8% formaldehyde in PBS and incubated an additional 5 minutes. We permeabilized the fixed cells by applying 0.1% [v/v] Triton X-100 in PBS for 5 minutes and blocked with 5% [w/v] BSA in PBS/Glycine (0.1 M) for 30 minutes. For staining, we diluted directly labeled primary antibodies in PBS/Glycine (0.1 M) containing 5% BSA [w/v]. We incubated the samples for 1 h at room temperature before washing six times with PBS to remove any unbound labels. For dual-color labeling of Mic10 and Mic19 along with Mic60 we incubated the samples with primary antibodies against Mic10 or Mic19 over night at 4 °C. Afterwards, we incubated the samples with antibodies against Mic60 for 1 h at room temperature.

Sample mounting and imaging buffers

For active sample stabilization during MINFLUX acquisition, we added fiducial markers (gold nanorods, A12-25-980-CTAB-DIH-1-25, Nanopartz Inc., Loveland, CO, USA) to all samples. The supplied solution of gold nanorods was diluted 1:3 in single-molecule clean PBS (P4417 Sigma-Aldrich, St. Louis, MO, USA) and sonicated for 5–10 minutes. The coverslips were incubated at room temperature with 100–500 µl of the nanorod solution for 5–15 minutes. Floating nanorods were removed by washing the sample 4–5 times with PBS. We filled single-welled microscope slides with the imaging buffer solution, mounted coverslips on top, removed excess of the buffer solution and sealed the samples with picodent twinsil speed 22 (picodent Dental-Produktions- und Vertriebs-GmbH, Wipperfürth, Germany) to prevent air exchange. We used a standard STORM imaging buffer containing 0.4 mg/ml glucose oxidase (G2133, Sigma Aldrich, St. Louis, MO, USA), 64 µg/ml catalase (C100-50MG, Sigma Aldrich, St. Louis, MO, USA), 50 mM TRIS/HCl pH 8.0/8.5, 10 mM NaCl, 10–200 mM cysteamine hydrochloride (MEA) (M6500, Sigma Aldrich, St. Louis, MO, USA) and 10% [w/v] glucose.

MINFLUX imaging

Data acquisition

For MINFLUX imaging, we used the optical microscope as previously described (4). In brief, the confocal part of the microscope enabled arbitrary wavefront phase control of the excitation beam with a spatial light modulator (LCOS-SLM X13267-06, Hamamatsu Photonics Deutschland GmbH, Herrsching am Ammersee, Germany) and fast deflection (xyz) using electro-optic deflectors (M-311-A, Conoptics Inc., Danbury, CT, USA and KLMS2D0700-00 KTN varifocal lens module, NTT Advanced Technology Corporation, Omiyacho Saiwai-ku, Kawasaki-shi, Japan). Electro-optic modulators (LM 0202 P 5W, Qioptiq Photonics GmbH Co. KG, Göttingen, Germany) provided fast on- and off-switching of the excitation light, whereas acousto-optic tunable filters (AOTFnC VIS-TN or AOTFnC 400.650-TN, AA Sa, Orsay, France) were used for power modulation and wavelength selection. These measures also allowed targeting the 3D doughnut-beam (5) of 642 nm wavelength (VFL-P-1500-642, MPB Communications Inc., Pointe-Claire, Quebec, Canada) to a set of positions as close as possible to a single molecule. A piezo-based tip-tilt mirror (PSH-10/2 piezosystem jena GmbH, Jena, Germany) additionally scanned the MINFLUX pattern to acquire the molecule positions in micrometer-sized fields of view. We conditionally activated single Alexa Fluor 647, CF660C or CF680 molecules using a coaligned, focused activation beam of 405 nm wavelength (405-50-COL-004, Oxxius, Lannion, France). The light was focused on the sample using a 1.4 NA oil objective lens (HC PL APO 100x/1.40 Oil CS2, Leica Microsystems GmbH, Wetzlar, Germany). The same objective lens collected the emitted fluorescence light. For multi-color imaging, we split the spectrum of the spatially filtered fluorescence (pinhole size 500 nm in the sample) at about 685 nm (FF685-Di02, Semrock Inc., Rochester, NY, USA) and detected both spectral fractions on avalanche photo-diodes (SPCM-AQRH-13-TR, Excelitas Technologies, Waltham, MA, USA). The region of interest was selected from a widefield EMCCD camera recording (Ixon EMCCD DU897-BV, Andor Technology Ltd., Belfast, UK) at 488 nm or 640 nm excitation. To ensure homogenous coverage of the area with the scanned activation beam, we chose scanning points in a distance of 200–250 nm within an arbitrarily shaped scan region. The system was actively stabilized using the total internal reflection of an infrared beam (905 nm illumination, LuxX®905-150, Omicron-Laserage, Laserprodukte GmbH, Rodgau-Dudenhofen, Germany) for axial position monitoring. The dark-field image of scattering gold nanorods (950–1000 nm illumination, Koheras SuperK Extreme, NKT Photonics, Birkerød, Denmark) monitored the position of the sample in the lateral direction. A PID controller repositioned the piezo-driven sample stage to ensure nanometer stability of the sample during MINFLUX acquisition. To cover extended regions with high photon-efficiency, we used the previously described iterative MINFLUX approach (4). We also used a field programmable gate array (FPGA, NI USB-7856R, National Instruments, Austin, TX, USA) for estimating the molecule position online and to subsequently reposition and shrink the MINFLUX

targeted coordinate pattern (TCP). We used the previously described iteration scheme for 3D MINFLUX imaging together with a modified least mean square estimator with optimized parameters. We controlled all hardware components and acquisition parameters using custom software written in Labview 2016 (National Instruments, Austin, TX, USA). We validated the microscope performance on a daily basis using fluorescent microspheres as described before (4).

Data analysis

The time traces of the detected photon counts were analyzed in steps as previously described and implemented in Matlab code (4). Briefly, to separate time frames of molecular emission from background, we segmented the traces employing a three-state Hidden-Markov model of the fluorescence emission. For reliable assessment of the localization precision, single emission events were split into sub-traces of 2000 photons; thus, we obtained several localizations per molecule.

A grid-search-based maximum-likelihood estimator delivered the molecule position and the signal-to-background ratio based on the photon counts collected for all coordinates targeted by the beam, i.e. the complete TCP, within the selected time frame.

The counts from both spectral detection channels were added for localization. To classify the emitter species, we added up photons from all target positions, and compared the photon totals on the two spectral channels. We included all iterations in the classification by performing a principal component analysis on the probability of photon detection on the blue-shifted channel of all iterations and localizations. We manually selected the classification threshold using the distribution of the first principal component so that spectral cross-talk was minimal (see Fig. S6).

During imaging, the FPGA automatically reacted on the appearance of molecular emission by subsequently turning off the activation light and starting the iterative MINFLUX localization. As we chose a low static photon count rate to distinguish background from fluorescence, we occasionally also reacted to fluctuations in the background counts. We excluded localizations due to background from display and further analysis based on three filters. First, we omitted localizations for which the gridsearch-based estimator fell to a border pixel in one of the four grid steps (Exitflag MLE<0.25). Further, we discarded localizations separated by more than 34.5 nm from the center of the TCP in the last iteration because background contributions usually delivered localizations far away from the TCP center. We omitted localizations containing less than 1013 photons. The histograms used for filtering are displayed in Fig. S6 and Fig. S7 for a dual-color acquisition and a single-color acquisition, respectively.

We estimated the experimental localization precision by co-aligning the mean value of all localization groups obtained from individual emission bursts. We fitted the resulting histogram with a Gaussian function to estimate the localization precision (see Fig. 1B). We only used localization clouds containing at least five localizations to avoid underestimating the localization error due to a statistical bias. This approach resulted in an average of 10 localizations per emission burst corresponding to 20,000–30,000 photons.

We further developed the three-step unsupervised clustering algorithm *dbscan2* to re-assign filtered localizations to individual fluorescent molecules. In the first two steps, the density-based clustering algorithm *dbscan* (6) (density-based spatial clustering of applications with noise, Matlab function DBSCAN) was used to pre-group localization clouds. Each of the *dbscan* steps was based on a search radius (*eps1* and *eps2*, respectively) and a localization count threshold (*minPts1* and *minPts2*, respectively). If at least *minPts* localization were found in the sphere of radius *eps* around a randomly chosen localization, all localizations in the sphere were assigned to the same localization cloud. For the molecular assignment of localizations we used *eps1*=10 nm, *eps2*=6 nm and *minPts1*=*minPts2*=4 throughout this work. In a last step, an expectation maximization using a Gaussian mixture model (Matlab function gmdistribution) refined the assignment by exploiting the knowledge that the spatial distribution of localizations originating from a single molecule is well-described by a Gaussian function.

We chose the mean values of the localizations in each cluster identified by the second *dbscan* step as the mean values of the individual Gaussian components in the mixture model. We pre-defined the spread σ_{GMM} of the 3D Gaussian functions in the mixture model. This parameter did not influence the assignment result because the surface of equal assignment probability of two Gaussian functions is independent of the numerical value of the spread itself as long as the spread

is equal for both functions. For extracting larger localization arrangements, we empirically optimized all *dbSCAN2* parameters as stated in the main text.

For display, we convolved the localizations with a 3D Gaussian kernel of width $\sigma=5$ nm. We used the square-root of the normalized image to avoid dominance of molecules with many emission events. We rendered the resulting volumes with voxels of side length 2.5 nm using the microscopy image analysis software Imaris (Bitplane AG, Zurich, Switzerland).

Electron tomography

For examination via transmission electron microscopy, U-2 OS cells were seeded on ACLAR slides (50425, Electron Microscopy Sciences, Hatfield, PA, USA) at a density of approximately 70 %. Cells were immobilized with freshly prepared and pre-warmed 2.5 % glutaraldehyde in 0.1 M phosphate buffer (pH 7.4). Fixation took place for one hour at room temperature and was completed at 4 °C over night. For secondary fixation and staining we first placed the cells in a solution containing 1 % osmium tetroxide and 1.5 % potassium-hexacyanoferrate (II) in 0.1 M phosphate buffer (pH 7.4) for one hour at room temperature. Without washing, the samples were then incubated in 1 % osmium tetroxide in 0.1 M phosphate buffer (pH 7.4) for an additional hour at room temperature. After 4 washing steps with double distilled water (5 minutes each), samples were placed in a solution consisting of 0.02 M lead nitrate and 0.03 M aspartic acid in double distilled water adjusted with sodium hydroxide to pH 5.5 and were kept in the solution at 60 °C for one hour. Subsequently, we washed the samples with double distilled water 3 times for 5 minutes each. The samples were dehydrated in a graded series of ethanol (30, 50, 75 and 100 %, 5 minutes each) with a final dehydration in propylene oxide for 5 minutes at room temperature prior to resin infiltration with a 1:1 mixture of propylene oxide and EPON (Embed-812, 14121, Electron Microscopy Sciences, Hatfield, PA, USA) for one hour and two fresh replacements of 100 % EPON (first for 1 hour, second over night at 4 °C). For the final embedding, the samples were covered with BEEM capsules (70000, Electron Microscopy Sciences, Hatfield, PA, USA) filled with fresh EPON resin and cured in an oven at 60 °C for 48 hours. We placed sections of 230 nm thickness (sections were prepared in parallel to the growth surface of the cells) on pioloform-coated slot grids (S2010-NOTCH, Electron Microscopy Sciences, Hatfield, PA, USA), covered with 10 nm protein-A gold, sputter-coated with carbon and then examined in a transmission electron microscope (Talos L120C TEM, Thermo Fischer Scientific, Waltham, MA, USA) operated at 120 kV. We acquired tilt series using a Saxton Scheme. We processed the final images and aligned and reconstructed the data using the IMOD software including the etomo package.

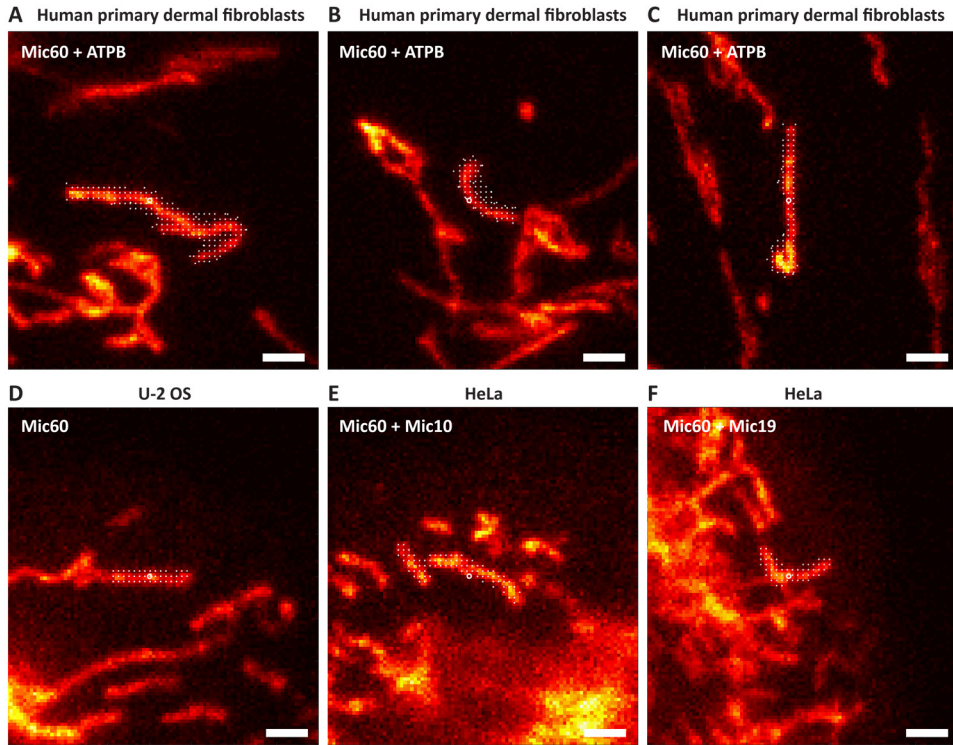


Fig. S1: Widefield images of regions acquired with MINFLUX nanoscopy.

A–C Human dermal fibroblasts — ATPB and Mic60 labeled using primary antibodies conjugated to Alexa Fluor 647 and CF660C respectively. The center of the available scanning region (white circles) and the MINFLUX scan points (white dots) are shown. Widefield excitation at 640 nm. MINFLUX data are shown in Fig. 1A and Mov. S1 (A), Fig. S2A and Mov. S2–S3 (B), Fig. S2B and Mov. S4–S5 (C), respectively. **D** U-2 OS cell — Mic60 labeled with primary antibodies conjugated to Alexa Fluor 647. MINFLUX data shown in Fig. 3A and Mov. S6. **E–F** Mic10-TG HeLa cells — Mic60 and Mic10 (E) or Mic19 (F) labeled with primary antibodies conjugated to Alexa Fluor 647 and CF680, respectively. MINFLUX data shown in Fig. 4A (E) and Fig. 4B (F). Scale bars: 2 μ m (A–F).

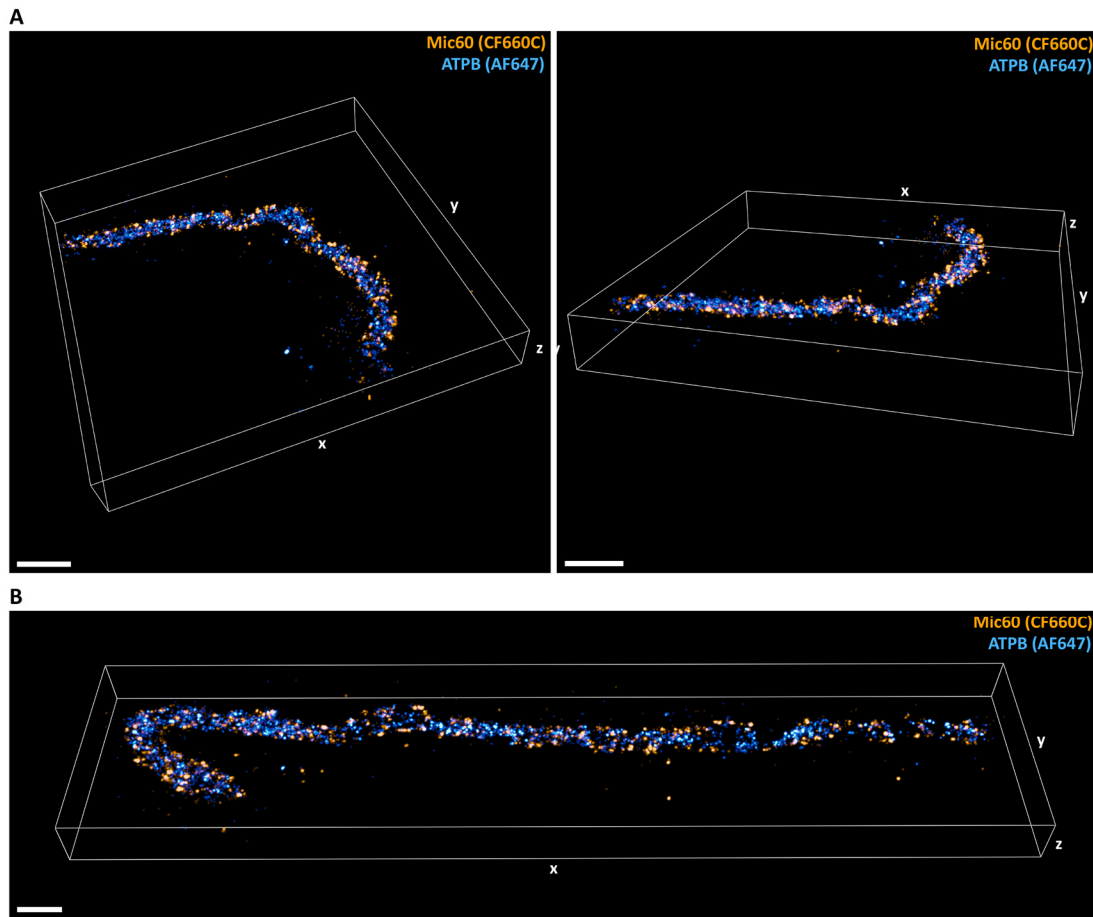


Fig. S2: 3D-MINFLUX recordings of mitochondria in primary human dermal fibroblasts.

Chemically fixed cells were labeled with antibodies against Mic60 conjugated to CF660C and against ATPB conjugated to Alexa Fluor 647, respectively. Animated renderings of the datasets are shown in Mov. S2–S3 (A) and Mov. S4–S5 (B). Scale bars: 500 nm (A–B).

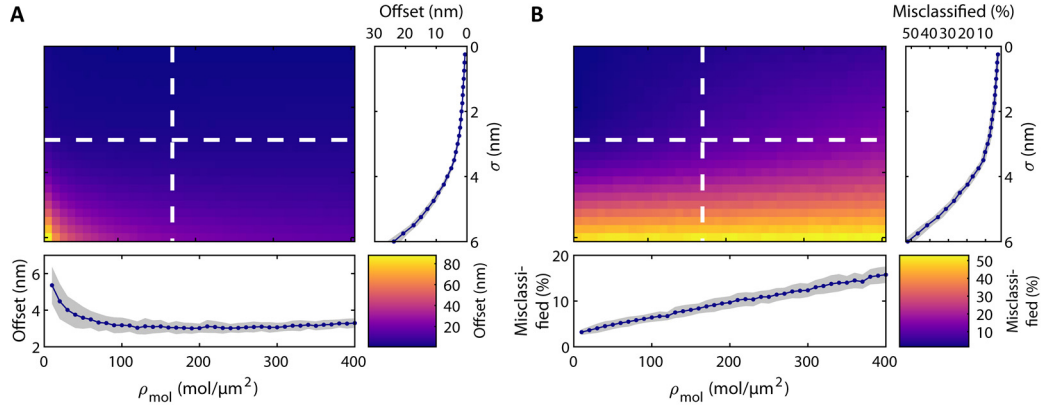


Fig. S3: Clustering error for a one-step *dbSCAN* algorithm.

Localizations were simulated as described in the main text using a cylinder diameter of 200 nm, a noise density of 400/ μm^3 and a Poissonian mean of 10 localizations per molecule, identical to Fig. 2. For clustering $\text{eps}=7.5$ nm and $\text{minPts}=4$ were used. **A** Average offset between identified molecules and closest ground-truth molecule versus molecular density ρ_{mol} and the 3D localization precision σ . Profiles along $\sigma=3$ nm and $\rho_{\text{mol}}=170$ molecules/ μm^2 with mean (blue line and dots) and standard deviation (gray area) of 50 simulations are shown. For $\sigma=3$ nm and $\rho_{\text{mol}}=170$ molecules/ μm^2 an error of 3 nm is obtained. **B** As in (A), but now showing the percentage of simulated molecules that were not assigned to exactly one cluster. For $\sigma=3$ nm and $\rho_{\text{mol}}=170$ molecules/ μm^2 an error of 8.83% is achieved.

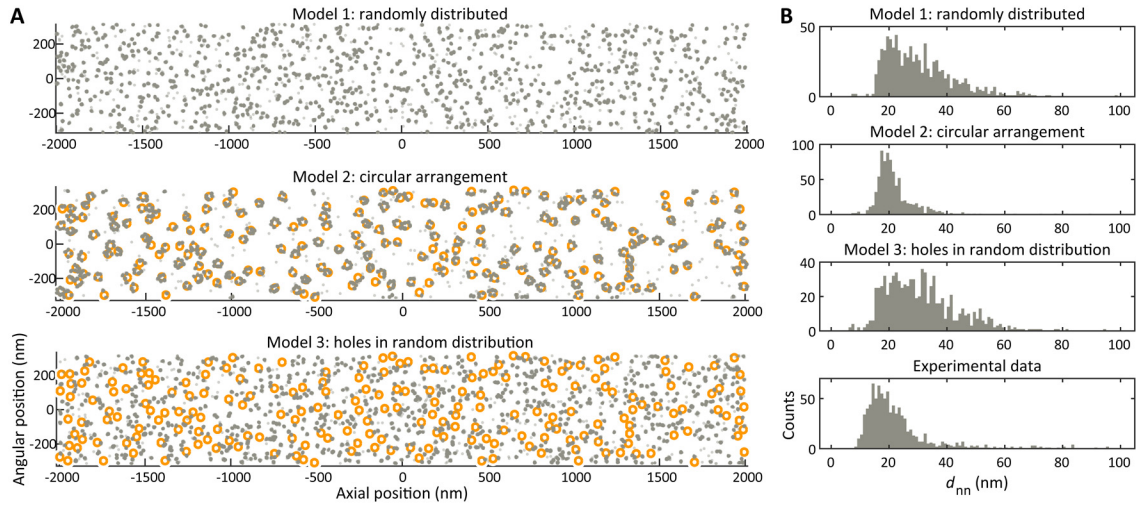


Fig. S4: Comparison of experimentally obtained Mic60 distribution with simulated models.

A Simulated localizations (gray dots) based on three different models. Model 1 assumes the molecules ($\rho \sim 350 \text{ molecules}/\mu\text{m}^2$) to be randomly distributed on a cylinder with a diameter of 200 nm using 18 localizations per molecule, a localization precision $\sigma=3 \text{ nm}$ and a noise density of 300 localizations/ μm^3 . In model 2, molecules are distributed within a Gaussian distribution of spread 5 nm of a circle line with diameter 40 nm (yellow circles), representing crista junctions. Seven molecules per junction and 60% labeling efficiency were assumed. All other parameters are as in model 1. Model 3 is based on randomly distributed molecule positions that cannot occupy the area of the crista junctions. The same parameters as before were used. **B** Histograms of nearest-neighbor distances between identified molecules using `dbSCAN2` ($\text{eps1}=10 \text{ nm}$, $\text{minPts1}=4$, $\text{eps2}=6 \text{ nm}$, $\text{minPts2}=4$, $\sigma_{\text{GMM}}=5 \text{ nm}$) for the three simulated models and the experimental data.

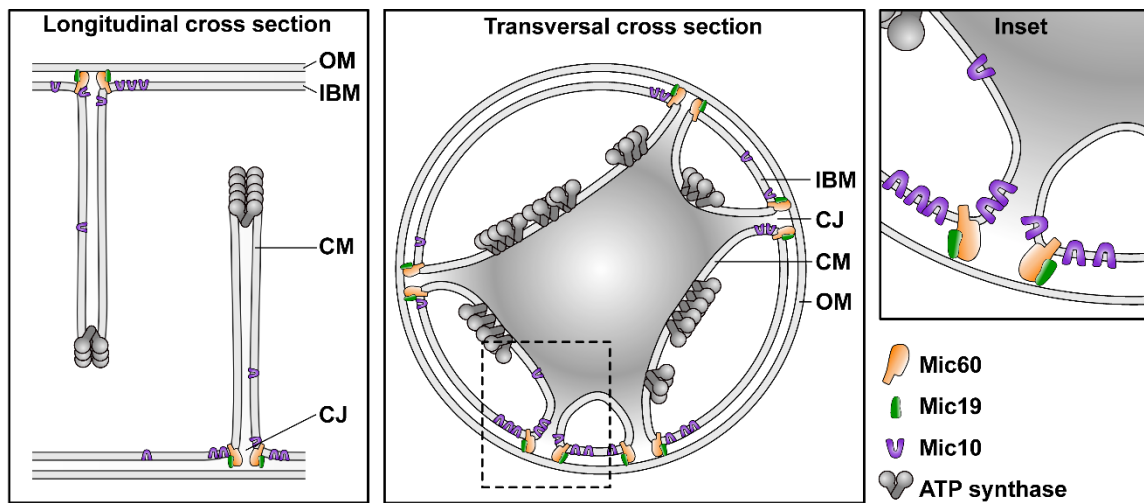


Fig. S5: Positioning of membrane proteins in mitochondria.

Cartoon illustrating the presumed localization of MICOS proteins and the mitochondrial F₁F₀-ATP synthase in mitochondria. Left: longitudinal cross section of the mitochondrial tubule. Center: transversal cross section of a lamellar crista. Right: inset with view onto a single crista junction. Abbreviations: OM: outer membrane, IBM: inner boundary membrane, CM: cristae membrane, CJ: crista junction.

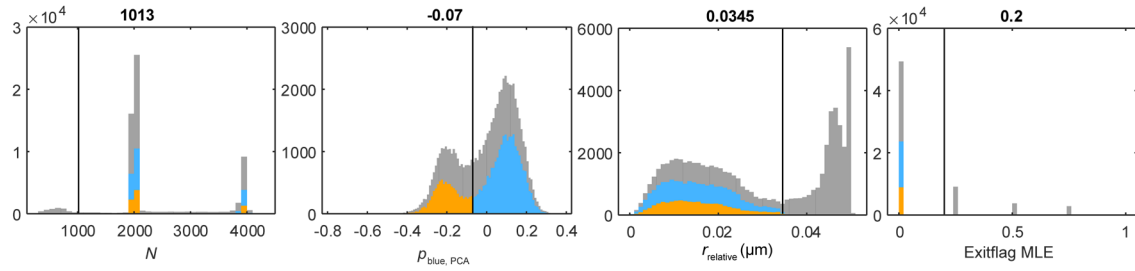


Fig. S6: Filter values and distributions for two-color 3D imaging in human dermal fibroblasts.

All distributions correspond to the data shown in Fig. 1A. Distribution of photon numbers in the last MINFLUX iteration N , first principal component of the count fraction on the detection channel for shorter wavelengths $p_{\text{blue,PCA}}$ used for species classification, distance of the localization to the TCP center in the last iteration r_{relative} and exitflag of the grid-search-based maximum-likelihood estimator. Exitflag values larger than 0 indicate coincidence of the localization result with one of the grid edges. In gray: full distribution. In orange: filtered distribution of CF660C. In blue: filtered distribution of Alexa Fluor 647. Filter values are indicated with black lines and on top of the histograms. Except for the spectral splitting, the same thresholds were used for dual-color images of Mic10 or Mic19 with Mic60 (Fig. 4).

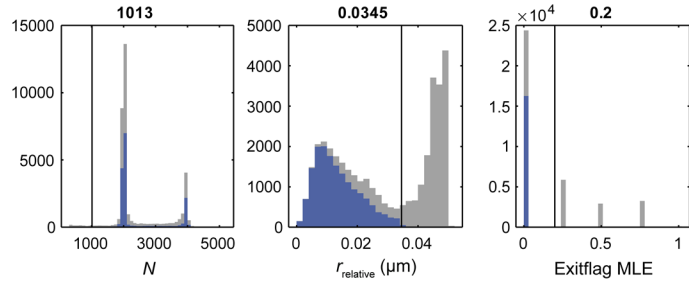


Fig. S7: Filter values and distributions for single-color Mic60 acquisition in U-2 OS cells.

All distributions correspond to the data shown in Fig. 3A. Distribution of photon numbers in the last iteration N , distance of the localization to the TCP center in the last iteration r_{relative} and exitflag of the grid-search-based maximum-likelihood estimator. Exitflag values larger than 0 indicate coincidence of the localization result with one of the grid edges. In gray: full distribution. In blue: filtered distribution of Alexa Fluor 647. Filter values are indicated with black lines and on top of the histograms.

Movie S1 (separate file): MINFLUX acquisition of a mitochondrion in a primary human dermal fibroblast as shown in Fig. 1A. Chemically fixed cells were labeled with antibodies against Mic60 conjugated to CF660C (orange) and against ATPB conjugated to Alexa Fluor 647 (blue), respectively.

Movie S2–S3 (separate file): MINFLUX acquisition of a mitochondrion in a primary human dermal fibroblast as shown in Fig. S2A. Chemically fixed cells were labeled with antibodies against Mic60 conjugated to CF660C (orange) and against ATPB conjugated to Alexa Fluor 647 (blue), respectively.

Movie S4–S5 (separate file): MINFLUX acquisition of a mitochondrion in a primary human dermal fibroblast as shown in Fig. S2B. Chemically fixed cells were labeled with antibodies against Mic60 conjugated to CF660C (orange) and against ATPB conjugated to Alexa Fluor 647 (blue), respectively.

Movie S6 (separate file): MINFLUX acquisition of Mic60 in a U-2 OS cell as shown in Fig. 3A. Chemically fixed cells were labeled with antibodies against Mic60 conjugated to Alexa Fluor 647. Axial positions> of the localizations are color-coded.

Movie S7 (separate file): Electron tomography of mitochondrion in U-2 OS cell as shown in Fig. 3C–D. Reconstruction of mitochondrial membranes with OM (transparent), matrix-facing side of the IM (dark blue) and IM facing towards intermembrane space (light blue).

SI References

1. J. Gruber, T. Lampe, M. Osborn, K. Weber, RNAi of FACE1 protease results in growth inhibition of human cells expressing lamin A: implications for Hutchinson-Gilford progeria syndrome. *J Cell Sci* **118**, 689-696 (2005).
2. T. Stephan *et al.*, MICOS assembly controls mitochondrial inner membrane remodeling and crista junction redistribution to mediate cristae formation. *EMBO J.*, e104105 (2020).
3. M. D. Ryan, A. M. Q. King, G. P. Thomas, Cleavage of foot-and-mouth disease virus polyprotein is mediated by residues located within a 19 amino acid sequence. *Journal of General Virology* **72**, 2727-2732 (1991).
4. K. C. Gwosch *et al.*, MINFLUX nanoscopy delivers 3D multicolor nanometer resolution in cells. *Nat. Methods* **17**, 217-224 (2020).
5. T. A. Klar, S. Jakobs, M. Dyba, A. Egner, S. W. Hell, Fluorescence microscopy with diffraction resolution barrier broken by stimulated emission. *Proceedings of the National Academy of Sciences* **97**, 8206-8210 (2000).
6. Ester M, Kriegel H-P, Jörg S, Xu X (1996) “A density-based algorithm for discovering clusters in large spatial databases with noise” in *Proceedings of the 2nd International Conference on Knowledge Discovery and Data Mining* (AAAI Press, Menlo Park, CA), pp 226–231.